

Supplementary Information: A Large Barrier Single-Molecule Magnet Without Magnetic Memory

Marcus J. Giansiracusa, Susan Al-Badran, Andreas K. Kostopoulos, George F. S. Whitehead, David Collison, Floriana Tuna, Richard E. P. Winpenny*, and Nicholas F. Chilton*

Contents:

S2-S6 Structural Information

S7 Molcas calculations

S8-S15 Magnetic data and CASSCF-SO results for **1**

S16-S19 Magnetic data for **1@1Y**

S20-S23 Magnetic data for **1d**

S24 Parameters for literature SMM compounds

S25 References

Synthesis

All reagents and solvents were purchased from commercial sources and used without further purification.

General procedure: 5,7-dimethyl-8-hydroxyquinoline (1 mmol) was added to a solution of DyCl₃.6H₂O (0.5 mmol) in methanol (20 mL). Then the resultant solution was heated to reflux for 3 hours. The solution was filtered and left for slow evaporation for 1 to 3 days, resulting in orange block shaped crystals suitable for X-ray crystallography.

The doped sample (Dy@Y) was prepared by mixing DyCl₃.6H₂O and YCl₃.6H₂O in a 1:19 molar ratio with DiMeQ in methanol according to the synthetic procedure used above.

[Dy(DiMeQ)₂(H₂O)Cl₃] (1). Quantities: 5,7-dimethyl-8-hydroxyquinoline (1 mmol, 0.173 g), DyCl₃.6H₂O (0.5 mmol, 0.188 g). Yield 0.152 g (48.25 % based on Dy).

Elemental analysis (%) calculated for C₂₂H₂₄DyN₂O₃Cl₃ (M_w = 633.31): C, 41.72; H, 3.82; N, 4.42; Cl, 16.79; Dy, 25.66; O, 7.59. Found: C, 41.44; H, 3.51; N, 4.34; Dy, 24.98.

[Dy_{0.07}Y_{0.93}(DiMeQ)₂(H₂O)Cl₃] (1@1Y). Quantities: 5,7-dimethyl-8-hydroxyquinoline (1 mmol, 0.173 g), DyCl₃.6H₂O (0.010 g, 0.025 mmol), YCl₃.6H₂O (0.144 gm, 0.475 mmol). Yield 0.17 g (60.4 % based on Y).

Elemental analysis (%) calculated for C₂₂H₂₄Y_{0.93}Dy_{0.07}N₂O₃Cl₃ (M_w = 564.85): C, 46.78; H, 4.28; N, 4.96; Cl, 18.83; Dy, 2.01; Y, 14.64; O, 8.50. Found: C, 45.90; H, 4.12; N, 4.57; Cl, 18.01; Dy, 1.76; Y, 13.86.

[Dy(DiMeQ^d)₂(D₂O)Cl₃] (1d). Quantities: 1d-5,7-dimethyl-8-hydroxyquinoline (1 mmol, 0.173 g, where the H of the hydroxyl group has been exchanged), DyCl₃.nD₂O (0.5 mmol, 0.188 g). Yield 0.148 g (46.98 % based on Dy).

Elemental analysis (%) calculated for C₂₂H₂₁D₃DyN₂O₃Cl₃ (M_w = 636.27): C, 41.53; H/D, 4.27; N, 4.40; Dy, 25.54; Cl, 16.72; O, 7.54. Found: C, 41.46; H, 4.02; N, 4.33; Dy, 24.93

[Y(DiMeQ)₂(H₂O)Cl₃] (1Y). Quantities: 5,7-dimethyl-8-hydroxyquinoline (1 mmol, 0.173 g), YCl₃.6H₂O (0.5 mmol, 0.151 g). Yield 0.146 g (52.51 % based on Y).

Elemental analysis (%) calculated for C₂₂H₂₄YN₂O₃Cl₃ (M_w = 559.70): C, 47.21; H, 4.32; N, 5.01; Cl, 19.00; Y, 15.88; O, 8.58. Found: C, 47.19; H, 4.20; N, 4.60; Cl, 18.36; Y, 14.99.

The C analysis of **1@1Y** is slightly outside the usually acceptable range; C can often be found low for complexes of heavier elements as some can be trapped rather than escaping as CO₂ on burning.

Crystallography

Data Collection. X-ray data were collected at a temperature of 150 K on an Oxford X'calibur 2 with an Atlas CCD detector with MoK_α radiation, ($\lambda = 0.71073 \text{ \AA}$) and equipped with an Oxford Cryosystem Cobra nitrogen flow gas system. Data was measured using CrysAlisPro suite.

Crystal structure determinations and refinements. X-ray data were processed and reduced using CrysAlisPro suite of programs. Absorption correction was performed using empirical methods based upon symmetry-equivalent reflections combined with measurements at different azimuthal angles.^{S1} The crystal structures were solved and refined against all F^2 values using the SHELXL through the Olex2 platform.^{S2} All the atoms were refined anisotropically. Hydrogen atoms were placed in calculated positions refined using idealized geometries (riding model) and assigned fixed isotropic displacement parameters.

CCDC 1864391 contains the supplementary crystallographic data for this paper. These data can be obtained free of charge *via* www.ccdc.cam.ac.uk/conts/retrieving.html (or from the Cambridge Crystallographic Data Centre, 12 Union Road, Cambridge CB21EZ, UK; fax: (+44)1223-336-033; or deposit@ccdc.cam.ac.uk).

Table S1: Crystallographic data for compound **1**.

(1)	
Chemical formula	C ₂₂ H ₂₄ Cl ₃ DyN ₂ O ₃
Formula Weight	633.28
Crystal system	Triclinic
Space group	P -1
a / Å	7.1571(16)
b / Å	9.297(2)
c / Å	10.210(3)
α / °	110.26(2)
β / °	106.28(2)
γ / °	92.557(18)
Volume / Å ³	604.1(3)
Z	1
ρ _{calc} g / cm ³	1.741
Temperature / K	150(2)
μ(MoKα)/mm ⁻¹	3.449
Goof on F ²	1.003
R1(>2σ(l)) ^a	0.0566
wR ₂ ^a	0.1108
Radiation (Å)	MoKα ($\lambda = 0.71073$)
2θ range for data collection/°	7.036 to 54.978
Index ranges	-8 ≤ h ≤ 9, -12 ≤ k ≤ 10, -12 ≤ l ≤ 13
Reflections collected	4488
Independent reflections	3550 [R _{int} = 0.0517, R _{sigma} = 0.1240]
Data/restraints/parameters	3550/37/150

Table S2: Continuous Shape Measures (CShM) calculations for compound **1**.^{s3}

Structure	HP-6	PPY-6	OC-6	TPR-6	JPPY-6
CShM	31.678	25.824	1.725	14.693	28.452

With HP-6 = Hexagon (D_{6h}), PPY-6 = Pentagonal pyramid (C_{5v}), OC-6 = Octahedron (O_h), TPR-6 = Trigonal prism (D_{3h}) and JPPY-5 = Johnson pentagonal pyramid (J2) (C_{5v}).

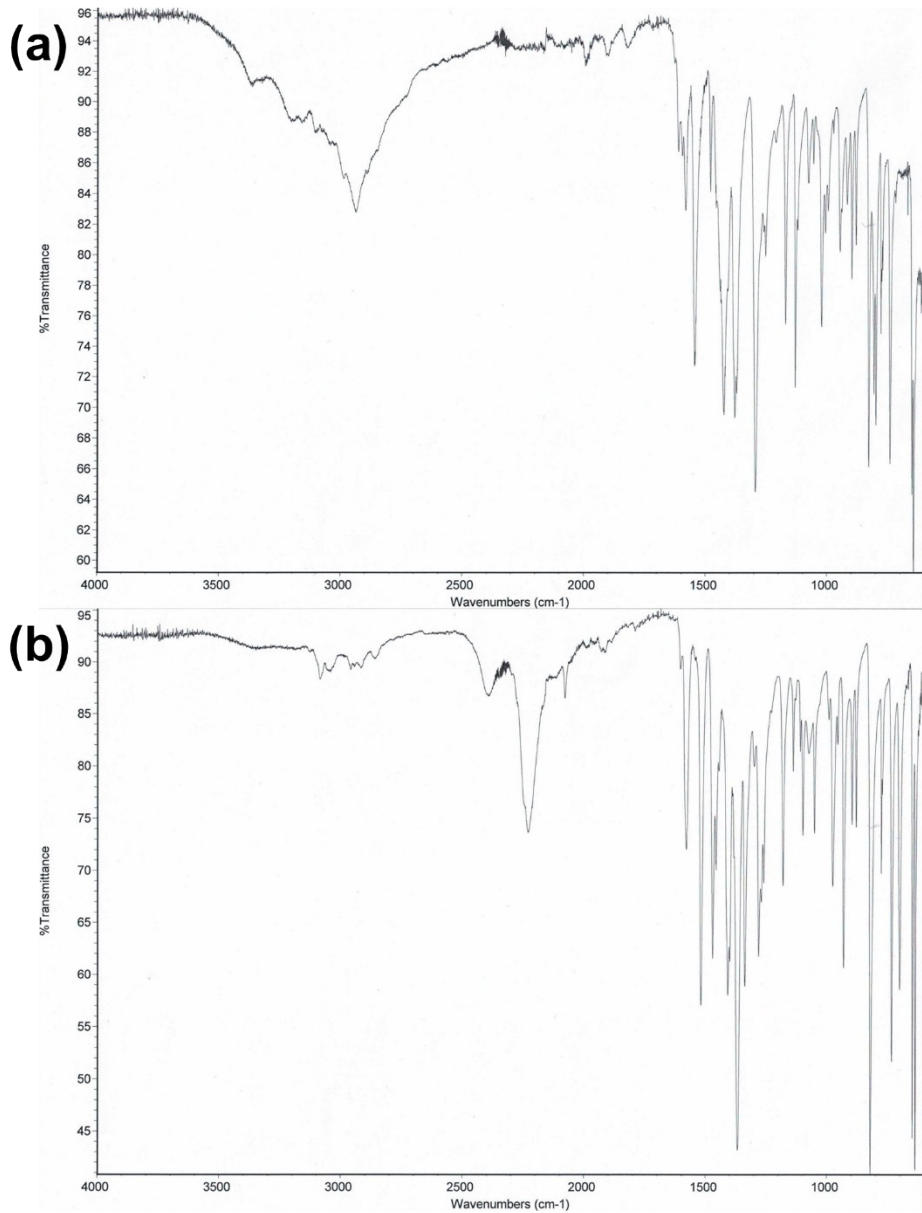


Figure S1. Infrared spectra recorded for (a) **1** and (b) **1d** as lightly ground powders using a Thermo Fisher Scientific Nicolet iS5 FTIR.

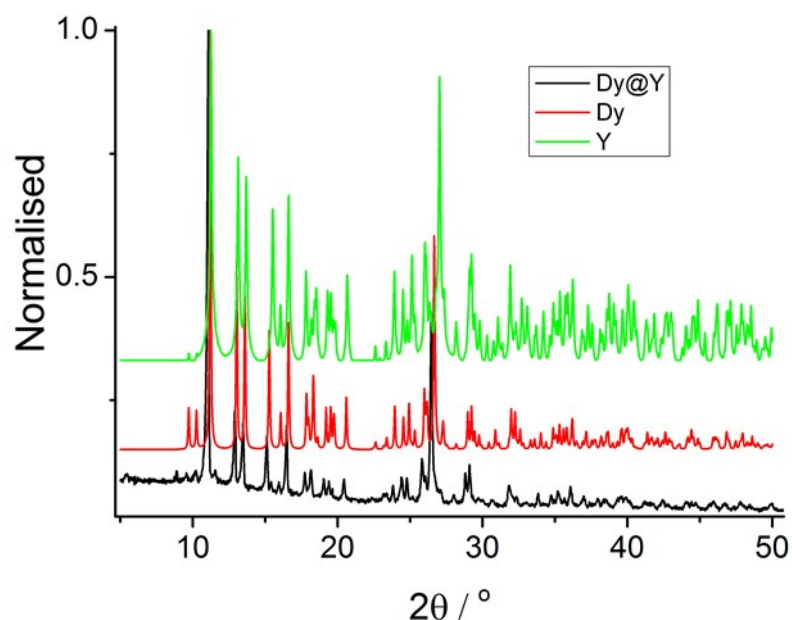


Figure S2. Top) Powder XRD performed on lightly ground samples **1@1Y** (black) compared to simulation of **1** (red) and **1Y** (green) samples calculated from single crystal XRD, to demonstrate phase purity of the bulk which was then subject to magnetic investigation.

Molcas Calculations

Complete active space self-consistent field spin orbit (CASSCF-SO) calculations were performed using MOLCAS 8.0^{S4} with the single crystal X-ray structure of an isolated [Dy(DiMeQ)₂Cl₃(H₂O)] molecule. The central Dy^{III} ion was described using the ANO-RCC VTZP quality basis, with the first coordination sphere described using VDZP and all other atoms using VDZ quality.^{S5} The two electron integrals were decomposed using the Cholesky approach with a threshold of 10⁻⁸. The active space incorporated the 9 active 4f electrons of Dy^{III} in the seven 4f orbitals. State-averaged CASSCF calculations were performed on the 21 sextet, 224 quartet and 490 doublet spin states, and then 21 sextets, 128 quartets and 130 doublets were mixed by SO coupling in the RASSI routine. The CFPs were extracted using Single_Aniso where the quantisation axis was the principal g_z -value of the ground Kramers doublet.^{S6}

Magnetic measurements

Variable temperature and field-dependent magnetic moment data were recorded on a Quantum Design MPMS XL7 SQUID magnetometer. To avoid sample reorientation during measurements, ground samples were fixed if needed with a known amount of eicosane. Diamagnetic corrections were applied using tabulated Pascal constants and measurements were corrected for the effect of the blank sample holder (straw) and eicosane.

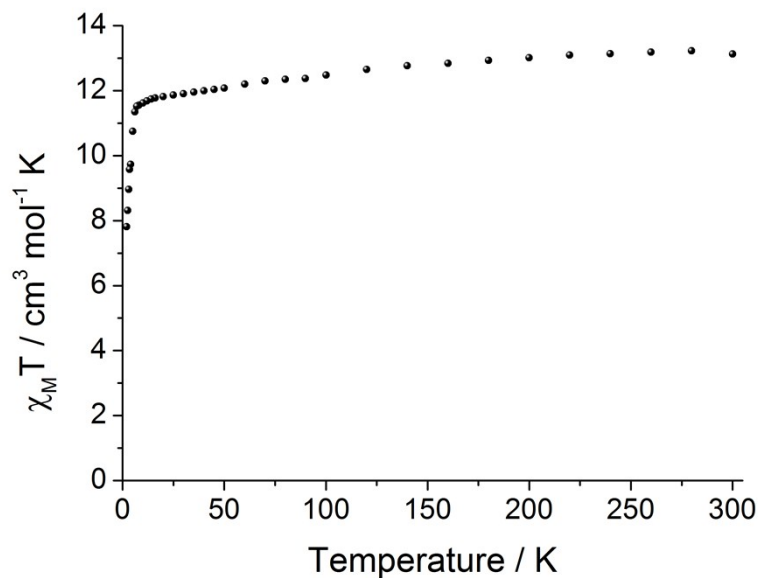


Figure S3. Magnetic susceptibility measurements of **1** performed with a 1000 Oe applied field in the temperature range 1.8 to 300 K.

The magnetic AC data were treated using the extended Debye model shown the equations below for a single relaxation process. Here the in-phase χ' is the real component of the susceptibility and the out-of-phase χ'' is the imaginary component. χ_s and χ_t represent the adiabatic and isothermal susceptibility, with the relaxation time τ and $\omega = 2\pi\nu$ representing the angular AC frequency.

$$\chi(\omega) = \chi_s + \frac{\chi_t - \chi_s}{1 + (i\omega\tau)^{(1-\alpha)}}$$

$$\chi' = \text{Re}[\chi(\omega)] = \chi_s + \frac{\chi_t - \chi_s}{1 + (\omega^2\tau^2)^{(1-\alpha)}}$$

$$\chi'' = \text{Im}[\chi(\omega)] = \frac{\omega\tau(\chi_T - \chi_S)}{1 + (\omega^2\tau^2)^{(1-\alpha)}}$$

For **1** and **1d**, magnetic AC data suitable for fitting were obtained between 2 and 68 K, however, due to the weaker signal from the dilute **1@1Y**, adequate signal was only obtained from 2 to 50 K. The fitting parameters are presented in Tables S3/6/7 for **1**, **1@1Y** and **1d** respectively. Large α parameters (>0.3) are obtained for the low temperature data for **1@1Y**, which likely originate from the weak signal.

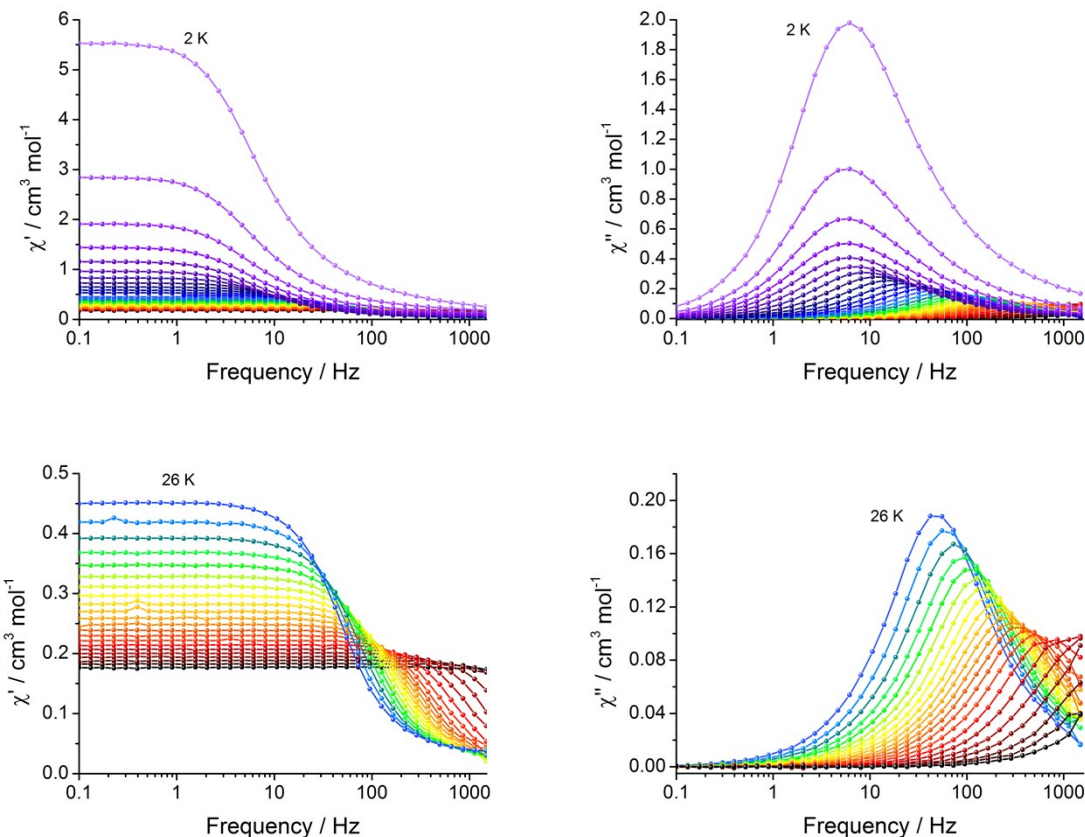


Figure S4. Alternating-current magnetic susceptibility data for **1** with the in-phase (left) and out-of-phase (right) signal depicted. For clarity the data have been truncated to fewer temperatures in the lower images so that clear frequency and temperature dependent peaks can be observed.

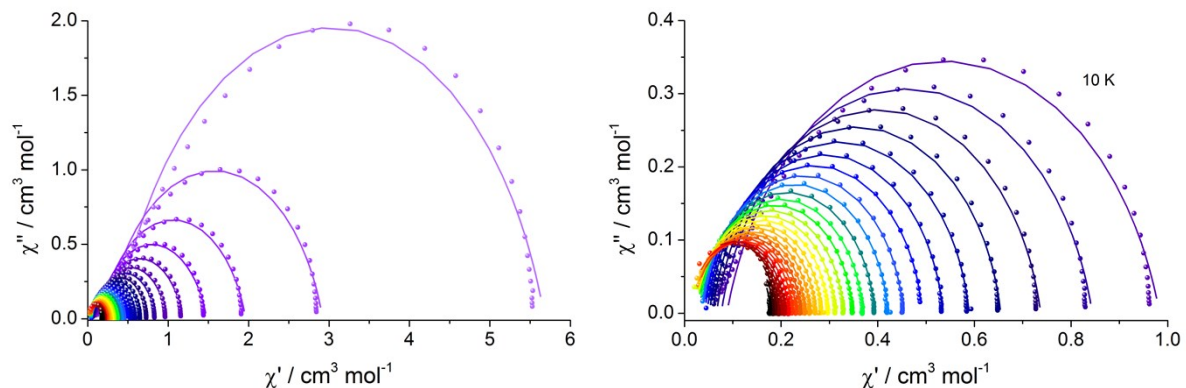


Figure S5. Left) Full Cole-Cole data from 2 to 68 K and **right)** 10 to 68 K showing the experimental data and fitted curves from equation S1 for **1**.

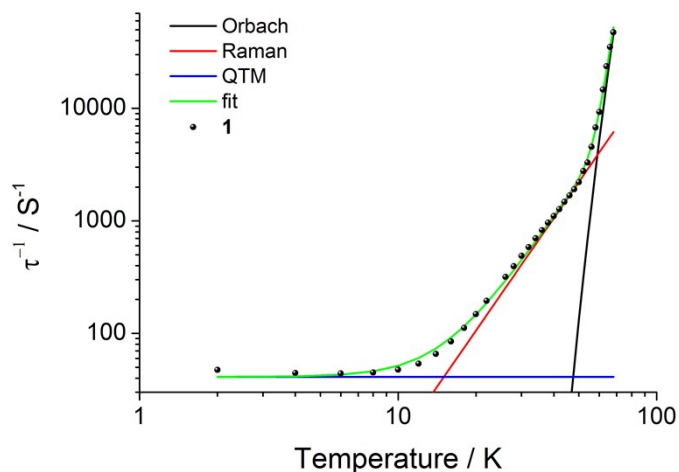


Figure S6. Fitted relaxation rate data for pure Dy sample **1** (■) using the Orbach, Raman and QTM parameters reported in main text. Orbach regime (black), Raman (red), QTM (blue) and overall fits (green) shown as solid lines.

Table S3. Fitting parameters for relaxation rate data of **1** showing value, standard error and confidence interval (low, high)

	Best Fit (Standard Error)	95 % Confidence Interval	
τ_0 (s)	$10^{-11.7(3)}$	3.51×10^{-13}	9.16×10^{-12}
U_{eff} (K)	1110(50)	1003	1214
C ($\times 10^{-3} \text{ s}^{-1} \text{ K}^{-n}$)	5(1)	2.63	7.60
n	3.32(7)	3.18	3.45
τ_{QTM} (s)	$2.44(9) \times 10^{-2}$	2.26×10^{-2}	2.62×10^{-2}

Table S4. Fitting parameters for **1** from Cole-Cole plots showing low values for α (<0.2) indicating a single relaxation mechanism.

T (K)	χ_s (cm ³ mol ⁻¹)	χ_T (cm ³ mol ⁻¹)	τ (s)	α	Residual
2	3.74×10^{-1}	5.68	2.11×10^{-2}	0.19	5.03×10^{-1}
4	2.31×10^{-1}	2.92	2.25×10^{-2}	0.19	1.08×10^{-1}
6	1.61×10^{-1}	1.96	2.27×10^{-2}	0.19	4.43×10^{-2}
8	1.23×10^{-1}	1.48	2.22×10^{-2}	0.19	2.53×10^{-2}
10	1.02×10^{-1}	1.18	2.10×10^{-2}	0.18	1.59×10^{-2}
12	8.77×10^{-2}	9.83×10^{-1}	1.86×10^{-2}	0.16	1.06×10^{-2}
14	7.59×10^{-2}	8.44×10^{-1}	1.52×10^{-2}	0.14	6.69×10^{-3}
16	6.65×10^{-2}	7.37×10^{-1}	1.18×10^{-2}	0.12	3.91×10^{-3}
18	5.87×10^{-2}	6.54×10^{-1}	8.93×10^{-3}	0.10	2.19×10^{-3}
20	5.19×10^{-2}	5.89×10^{-1}	6.74×10^{-3}	0.09	1.53×10^{-3}
22	4.72×10^{-2}	5.34×10^{-1}	5.14×10^{-3}	0.07	8.80×10^{-4}
24	4.25×10^{-2}	4.92×10^{-1}	4.01×10^{-3}	0.07	3.00×10^{-4}
26	3.84×10^{-2}	4.52×10^{-1}	3.15×10^{-3}	0.06	2.08×10^{-4}
28	3.56×10^{-2}	4.20×10^{-1}	2.53×10^{-3}	0.06	2.21×10^{-4}
30	3.13×10^{-2}	3.93×10^{-1}	2.05×10^{-3}	0.06	3.39×10^{-4}
32	3.15×10^{-2}	3.69×10^{-1}	1.71×10^{-3}	0.05	1.77×10^{-4}
34	2.72×10^{-2}	3.48×10^{-1}	1.43×10^{-3}	0.05	1.70×10^{-4}
36	2.49×10^{-2}	3.29×10^{-1}	1.21×10^{-3}	0.05	1.18×10^{-4}
38	2.31×10^{-2}	3.12×10^{-1}	1.04×10^{-3}	0.05	1.78×10^{-4}
40	2.47×10^{-2}	2.97×10^{-1}	9.05×10^{-4}	0.04	1.03×10^{-4}
42	2.28×10^{-2}	2.83×10^{-1}	7.85×10^{-4}	0.05	2.43×10^{-4}
44	1.73×10^{-2}	2.71×10^{-1}	6.78×10^{-4}	0.05	1.61×10^{-4}
46	1.91×10^{-2}	2.59×10^{-1}	5.94×10^{-4}	0.05	2.68×10^{-4}
48	1.98×10^{-2}	2.49×10^{-1}	5.23×10^{-4}	0.03	1.18×10^{-4}
50	2.11×10^{-2}	2.39×10^{-1}	4.52×10^{-4}	0.03	9.82×10^{-5}
52	1.28×10^{-2}	2.31×10^{-1}	3.61×10^{-4}	0.04	1.66×10^{-4}
54	1.99×10^{-2}	2.22×10^{-1}	3.02×10^{-4}	0.02	6.28×10^{-5}
56	1.25×10^{-2}	2.15×10^{-1}	2.19×10^{-4}	0.02	7.11×10^{-5}
58	2.93×10^{-3}	2.07×10^{-1}	1.48×10^{-4}	0.03	1.03×10^{-4}
60	1.07×10^{-2}	2.00×10^{-1}	1.07×10^{-4}	0.01	3.51×10^{-5}
62	8.26×10^{-7}	1.94×10^{-1}	6.82×10^{-5}	0.00	3.53×10^{-5}
64	1.22×10^{-6}	1.88×10^{-1}	4.23×10^{-5}	0.00	7.94×10^{-5}
66	1.83×10^{-6}	1.83×10^{-1}	2.84×10^{-5}	0.00	6.95×10^{-5}
68	2.75×10^{-6}	1.77×10^{-1}	2.11×10^{-5}	0.00	8.00×10^{-5}

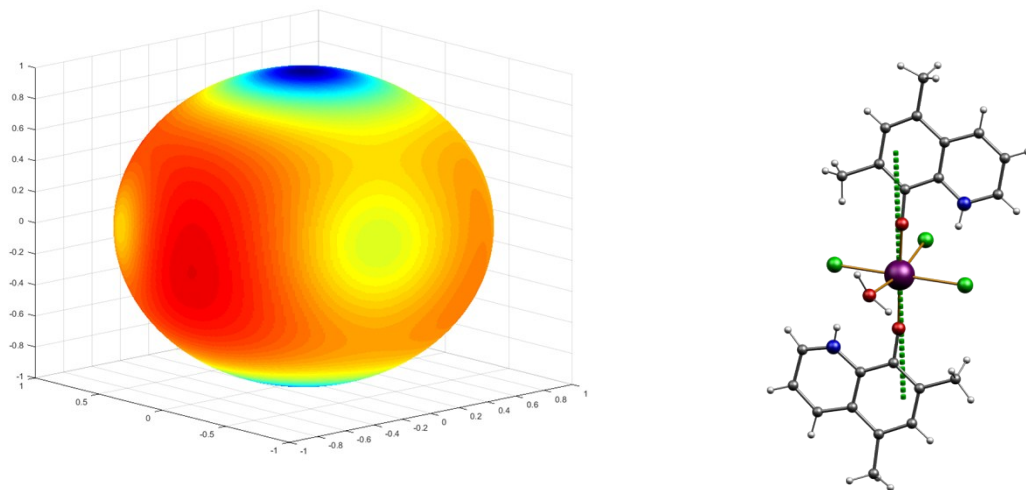


Figure S7. Left: Electrostatic potential calculation at 1 Å from the Dy ion centre, demonstrating the strong axial donor nature of the ligand environment. Scale with blue at -0.07 to red +0.02 V. Water molecules are described with a -2/3 charge for O and +1/3 charge for H. **Right:** Magellan^{S7} calculated easy axis for **1** showing the stabilisation of the $m_J = \pm 15/2$ ground state towards the phenoxide ligands. Magellan predicts an energy barrier of 1050 K (735.2 cm⁻¹) taking into account all charged atoms in the molecule and treating the water molecule as above.

Table S5. Wavefunction decomposition calculated in the basis of the principal axis of the ground doublet for **1**. The ground g_z orientation is defined by the principal g -value of the ground doublet, with the angle to subsequent g_z calculated relative to the ground state principal axis.

Energy (cm ⁻¹)	Energy (K)	g _x	g _y	g _z	g _z angle (degrees)	Wavefunction
0	0	0.00	0.00	19.86	--	98.3 % ±15/2⟩, 1.4 % ±13/2⟩
388	558	0.09	0.12	16.89	3.34	1.4 % ±15/2⟩, 95.6 % ±13/2⟩ 1.1 % ±11/2⟩, 1.1 % ±5/2⟩
656	944	1.82	3.35	12.39	12.56	80.0 % ±11/2⟩, 3.3 % ±7/2⟩, 1.7 % ±5/2⟩, 10.6 % ±3/2⟩, 2.9 % ±1/2⟩
761	1095	10.57	6.45	2.00	5.95	1.0 % ±13/2⟩, 10.8 % ±11/2⟩ 25.4 % ±9/2⟩, 4.6 % ±7/2⟩ 10.2 % ±5/2⟩, 7.2 % ±3/2⟩ 40.8 % ±1/2⟩
870	1252	0.98	2.85	11.98	75.53	4.7 % ±11/2⟩, 44.9 % ±9/2⟩, 15.9 % ±7/2⟩, 7.7 % ±5/2⟩, 21.8 % ±3/2⟩, 4.7 % ±1/2⟩
901	1296	0.24	3.01	15.01	86.85	1.8 % ±11/2⟩, 13.7 % ±9/2⟩ 8.9 % ±7/2⟩, 17.9 % ±5/2⟩ 30.4 % ±3/2⟩, 26.9 % ±1/2⟩
945	1359	1.15	2.72	14.36	78.40	8.7 % ±9/2⟩, 38.1 % ±7/2⟩ 32.8 % ±5/2⟩, 11.2 % ±3/2⟩ 8.6 % ±1/2⟩
994	1430	0.58	1.55	18.23	89.61	1.2 % ±11/2⟩, 6.5 % ±9/2⟩ 29.0 % ±7/2⟩, 28.5 % ±5/2⟩ 18.7 % ±3/2⟩, 15.9 % ±1/2⟩

Table S6. Crystal field parameters (including operator equivalent factors) in the basis of the principal axis of the ground doublet state for **1**, given in cm⁻¹.⁵⁶

	k	q	CFP
B	2	-2	4.62 x 10 ⁻¹
B	2	-1	7.02 x 10 ⁻¹
B	2	0	-5.00
B	2	1	6.53 x 10 ⁻²
B	2	2	1.23
B	4	-4	3.76 x 10 ⁻³
B	4	-3	1.61 x 10 ⁻²
B	4	-2	-7.13 x 10 ⁻⁴
B	4	-1	1.81 x 10 ⁻²
B	4	0	-1.10 x 10 ⁻²
B	4	1	-7.12 x 10 ⁻³
B	4	2	1.30 x 10 ⁻³
B	4	3	6.95 x 10 ⁻³
B	4	4	-3.39 x 10 ⁻²
B	6	-6	-6.07 x 10 ⁻⁵
B	6	-5	2.60 x 10 ⁻⁴
B	6	-4	2.46 x 10 ⁻⁵
B	6	-3	1.31 x 10 ⁻⁴
B	6	-2	-9.80 x 10 ⁻⁶
B	6	-1	-2.51 x 10 ⁻⁵
B	6	0	2.57 x 10 ⁻⁵
B	6	1	-1.28 x 10 ⁻⁵
B	6	2	-7.85 x 10 ⁻⁶
B	6	3	2.83 x 10 ⁻⁵
B	6	4	-1.83 x 10 ⁻⁴
B	6	5	-7.20 x 10 ⁻⁵
B	6	6	7.24 x 10 ⁻⁵

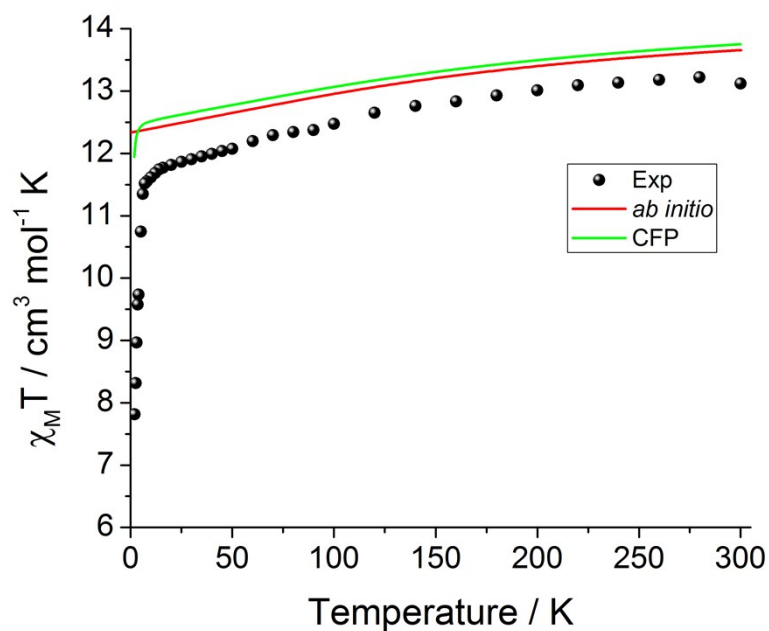


Figure S8. Magnetic susceptibility measurements of **1** performed with a 1000 Oe applied field in the temperature range 1.8 to 300 K, with theoretical *ab initio* simulated spectrum (red) and CFP simulated spectrum (green).

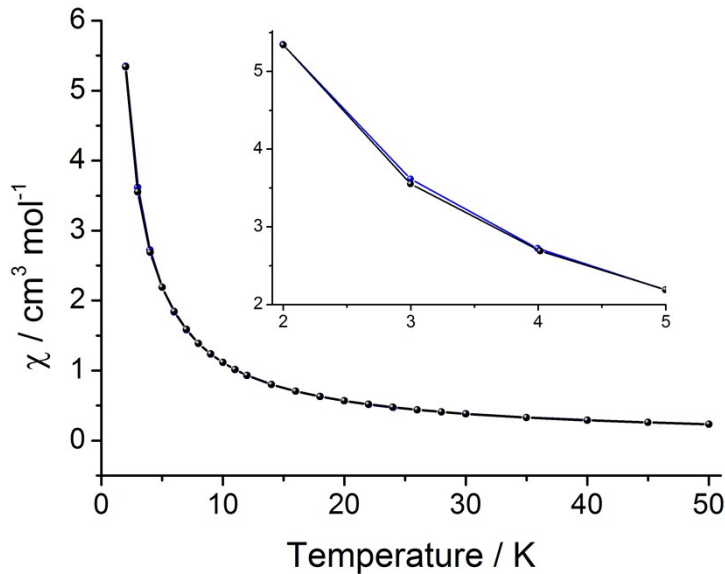


Figure S9. Zero-field cooled (blue) and field cooled (black) susceptibility data for **1** measured in a 100 Oe applied field, showing no separation (Sweep 0.3 K min⁻¹ below 12 K).

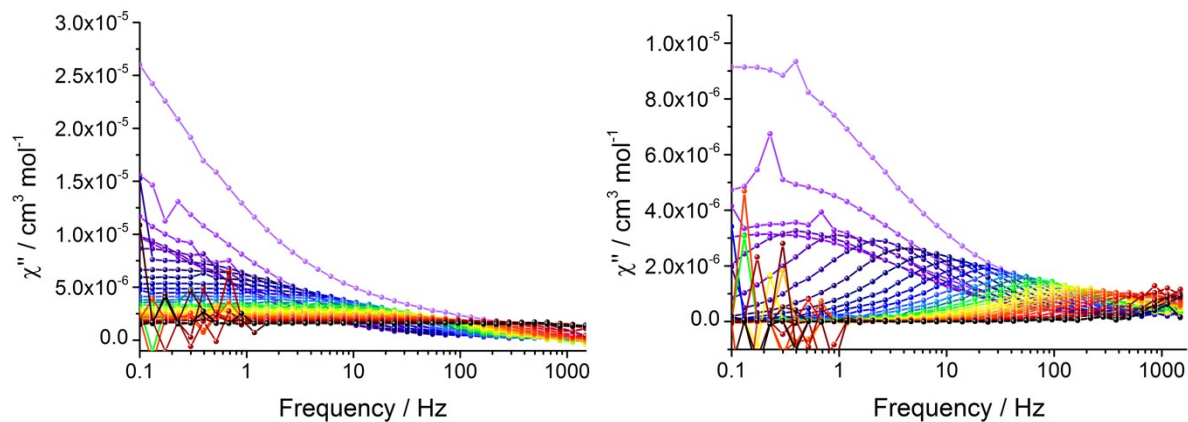


Figure S10. In-phase (**left**) and out-of-phase (**right**) susceptibility data for **1@1Y** from 2 to 68 K.

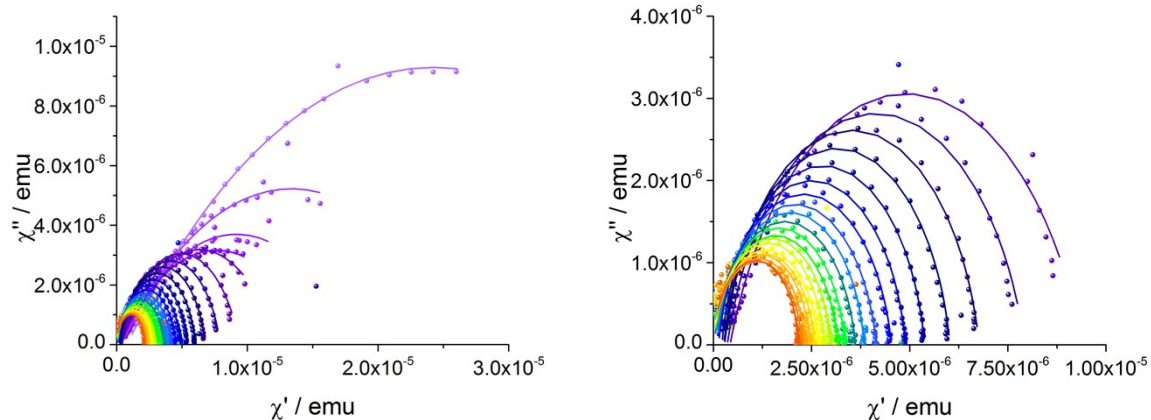


Figure S11. **Left)** Full Cole-Cole data for **1@1Y** from 2 to 50 K and **right)** restricted from 12 to 50 K because the quality of the data at higher temperatures did not allow reliable fits.

Table S7. Fitting parameters for relaxation rate data of **1@1Y** showing value, standard error and confidence interval (low, high), Orbach region is unobservable.

	Best Fit (Standard Error)	95 % Confidence Interval	
	1@1Y Fitting only (Figure 2 MS)		
C (x 10 ⁻⁴ s ⁻¹ K ⁻ⁿ)	4(1)	1.19	6.92
n	4.0(1)	3.78	4.20
τ_{QTM2} (s)	1.9(3)	1.22	2.59

Table S8. The fitting parameters for **1@1Y** from Cole-Cole plots (NOTE: values are in emu for the dilute sample as the paramagnetic sample mass is not directly measured). The α parameters are larger here likely due to the weaker signal from the dilute sample.

T (K)	χ_S (emu)	χ_T (emu)	τ (s)	α	Residual
2	8.20×10^{-7}	4.76×10^{-5}	1.20	0.52	2.91×10^{-12}
4	3.74×10^{-7}	2.64×10^{-5}	8.87×10^{-1}	0.51	9.70×10^{-12}
6	3.11×10^{-7}	1.80×10^{-5}	6.19×10^{-1}	0.50	2.64×10^{-12}
8	2.91×10^{-7}	1.50×10^{-5}	6.13×10^{-1}	0.48	3.60×10^{-13}
10	3.78×10^{-7}	1.23×10^{-5}	3.17×10^{-1}	0.37	8.67×10^{-13}
12	4.24×10^{-7}	9.40×10^{-6}	1.25×10^{-1}	0.24	1.76×10^{-12}
14	3.51×10^{-7}	7.93×10^{-6}	6.36×10^{-2}	0.19	3.79×10^{-12}
16	2.85×10^{-7}	6.77×10^{-6}	3.37×10^{-2}	0.14	6.05×10^{-13}
18	2.71×10^{-7}	6.02×10^{-6}	2.10×10^{-2}	0.12	4.83×10^{-13}
20	2.18×10^{-7}	5.38×10^{-6}	1.33×10^{-2}	0.11	3.36×10^{-13}
22	1.31×10^{-7}	4.89×10^{-6}	9.01×10^{-3}	0.11	4.13×10^{-13}
24	8.23×10^{-8}	4.53×10^{-6}	6.48×10^{-3}	0.12	1.19×10^{-11}
26	1.89×10^{-8}	4.15×10^{-6}	4.62×10^{-3}	0.12	9.64×10^{-13}
28	8.58×10^{-8}	3.84×10^{-6}	3.64×10^{-3}	0.10	2.38×10^{-13}
30	3.15×10^{-8}	3.62×10^{-6}	2.88×10^{-3}	0.11	1.84×10^{-12}
32	1.59×10^{-8}	3.35×10^{-6}	2.24×10^{-3}	0.10	1.73×10^{-13}
34	2.31×10^{-14}	3.17×10^{-6}	1.84×10^{-3}	0.11	9.66×10^{-12}
36	4.26×10^{-14}	2.98×10^{-6}	1.54×10^{-3}	0.09	5.53×10^{-13}
38	6.31×10^{-14}	2.82×10^{-6}	1.26×10^{-3}	0.08	3.50×10^{-13}
40	8.25×10^{-14}	2.68×10^{-6}	1.07×10^{-3}	0.09	3.84×10^{-12}
42	1.26×10^{-13}	2.58×10^{-6}	9.39×10^{-4}	0.09	4.69×10^{-13}
44	1.61×10^{-13}	2.46×10^{-6}	8.31×10^{-4}	0.07	5.56×10^{-12}
46	2.33×10^{-13}	2.33×10^{-6}	6.96×10^{-4}	0.06	1.93×10^{-12}
48	3.23×10^{-13}	2.25×10^{-6}	5.94×10^{-4}	0.06	2.11×10^{-13}
50	4.44×10^{-13}	2.16×10^{-6}	5.14×10^{-4}	0.03	5.59×10^{-12}

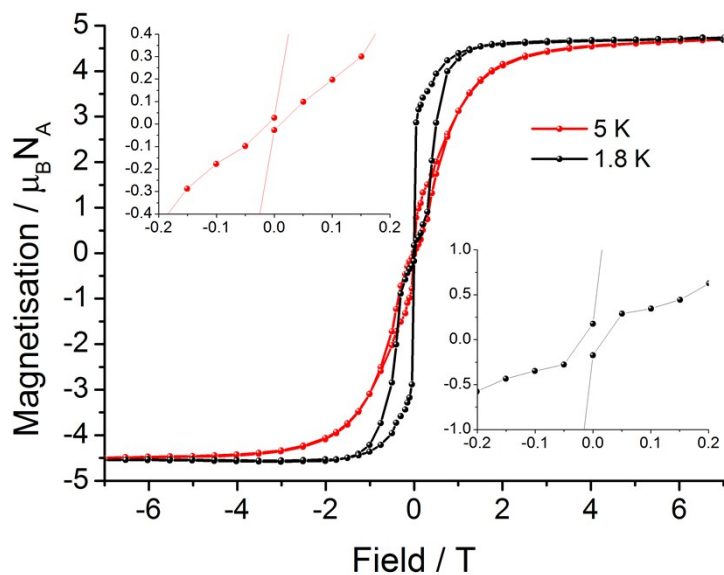


Figure S12. Magnetic hysteresis measurement performed on **1@1Y** at 1.8 and 5 K with expansion around zero field in insets, showing the presence of open hysteresis with sweep rate of *ca.* 15 Oe s⁻¹ when passing 0 T. Saturation value for dilute sample was scaled to 1, equivalent to an 8 % concentration of Dy and consistent with the elemental composition determined.

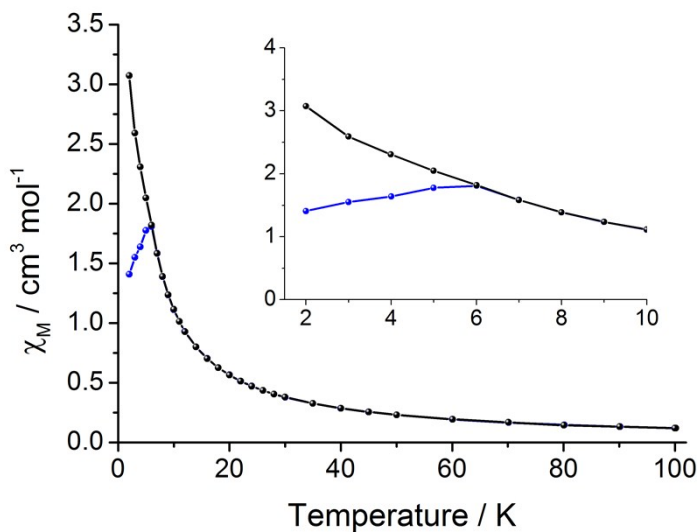


Figure S13. Zero-field cooled (blue) and field cooled (black) susceptibility data measured on **1@1Y** in a 100 Oe applied field, showing bifurcation below 6 K, and the inset is an expansion of the 2 – 10 K region (Sweep 0.3 K min⁻¹ below 12 K).

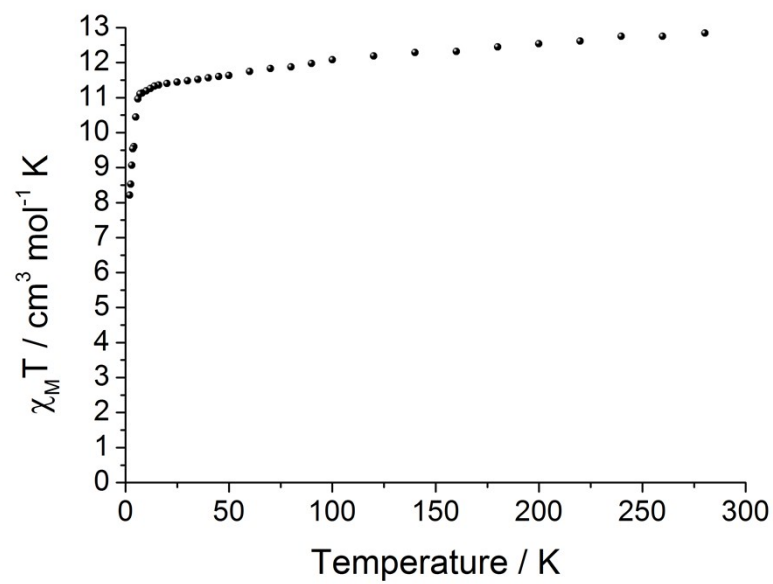


Figure S14. Magnetic susceptibility measurements of **1d** performed with a 1000 Oe applied field in the temperature range 1.8 to 300 K.

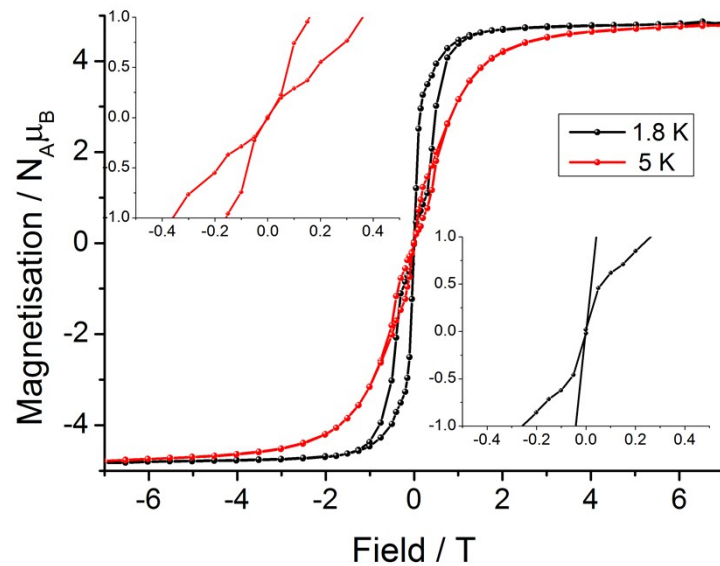


Figure S15. Magnetic hysteresis measurement performed on **1d** at 1.8 and 5 K with expansion around 0 field in insets, showing no open hysteresis with sweep rate of ca. 15 Oe s⁻¹ when passing 0 T.

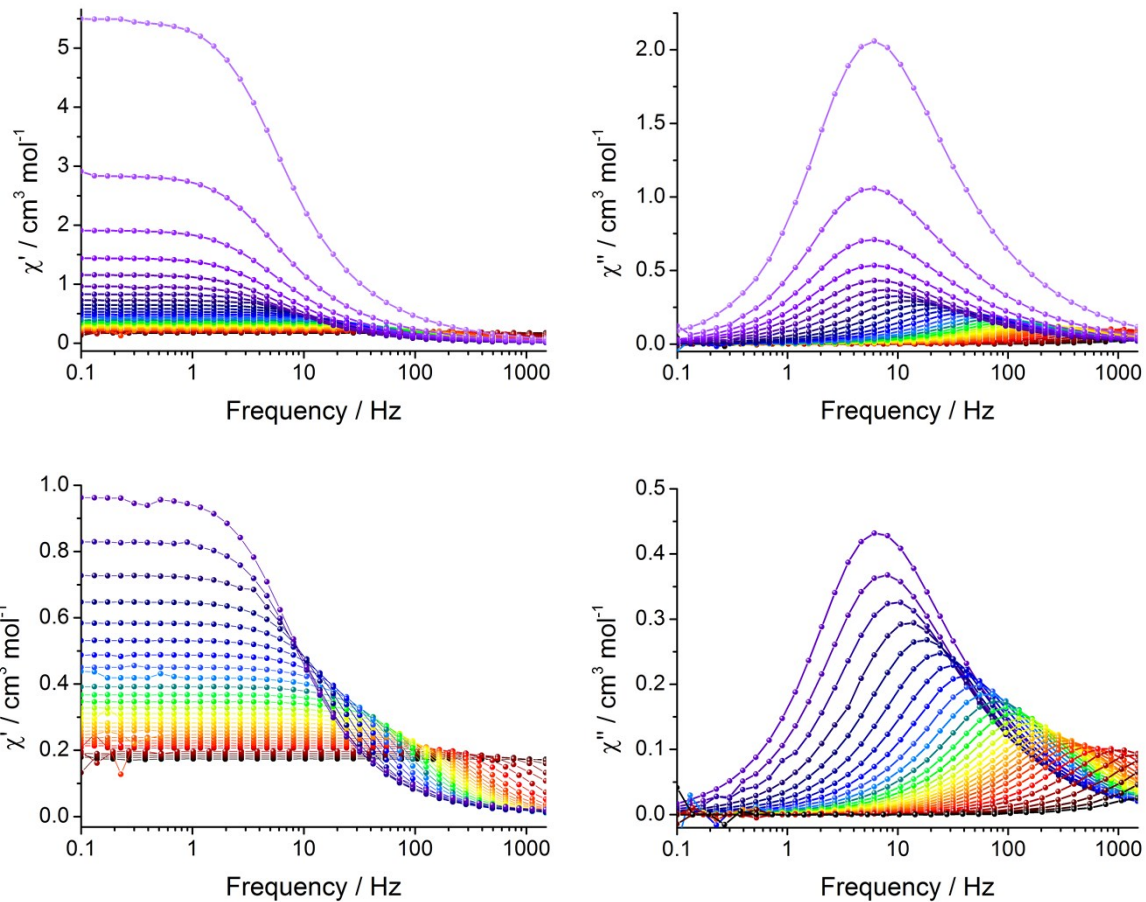


Figure S16. In-phase (**left**) and out-of-phase (**right**) magnetic susceptibility data for **1d** from 2 to 68 K with expansion below from 10 to 68 K.

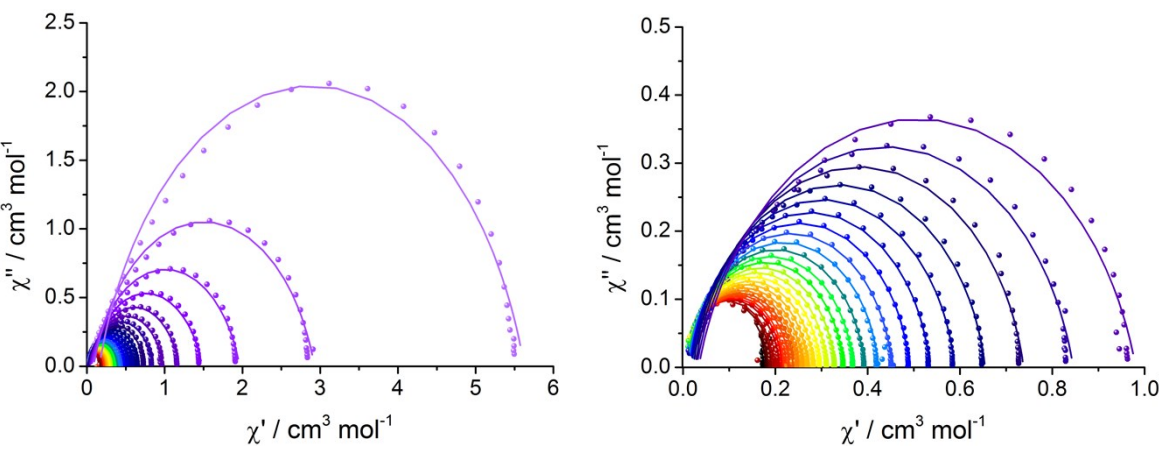


Figure S17. **Left)** Full Cole-Cole data for **1d** and **right)** expansion restricted from 12 to 68 K.

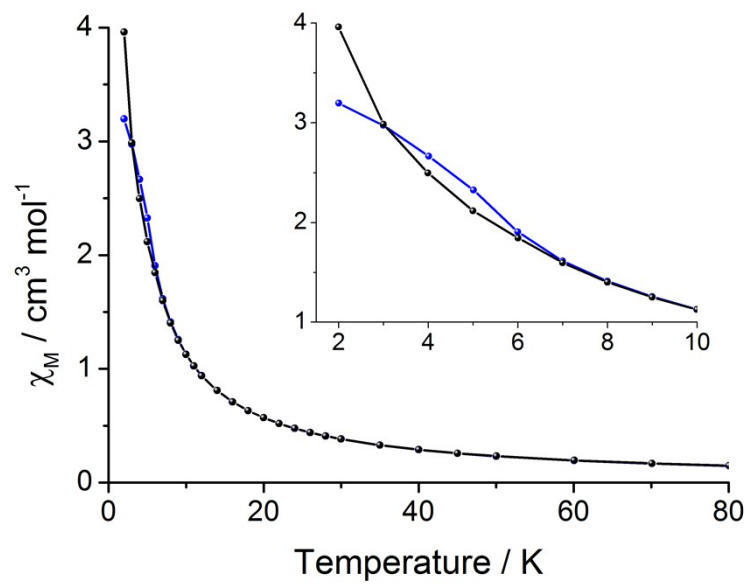


Figure S18. Zero-field cooled (blue) and field cooled (black) susceptibility data measured on **1d** in a 100 Oe applied field, showing slight separation below 6 K however, no observable peak in the ZFC trace (Sweep 0.3 K min^{-1} below 12 K).

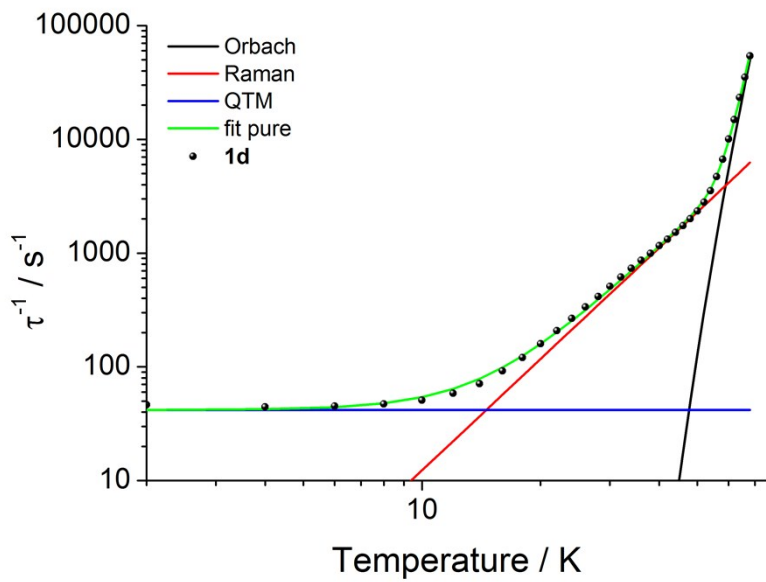


Figure S19. Fitting of relaxation rate data for **1d** using equation 1 from main text, revealing almost identical parameters to **1**. $U_{\text{eff}} = 1130(40)$ K with $\tau_0 = 1.3 \times 10^{-12}$ ($10^{-11.9(3)}$) s, $C = 7(1) \times 10^{-3}$ $\text{s}^{-1} \text{K}^{-n}$, $n = 3.25(5)$ and $\tau_{QTM} = 0.0239(6)$ s.

Table S9. Fitting parameters for relaxation rate data of **1d** showing value, standard error and confidence interval (low, high)

	Best Fit (Standard Error)	95 % Confidence Interval	
t_0 (s)	$10^{-11.9(3)}$	3.90×10^{-13}	4.31×10^{-12}
U_{eff} (K)	1120(40)	1049	1204
C ($\times 10^{-3}$ $\text{s}^{-1} \text{K}^{-n}$)	7(1)	4.62	9.28
n	3.25(5)	3.15	3.34
τ_{QTM} (s)	$2.39(6) \times 10^{-2}$	2.26×10^{-2}	2.53×10^{-2}

Table S10. Fitting parameters for **1d** from Cole-Cole plots showing low values for α (<0.2) indicating a single relaxation mechanism.

T (K)	χ_s (cm ³ mol ⁻¹)	χ_T (cm ³ mol ⁻¹)	τ (s)	α	Residual
2	1.57 x 10 ⁻¹	5.62	2.16 x 10 ⁻²	0.18	3.70 x 10 ⁻¹
4	8.42 x 10 ⁻²	2.93	2.25 x 10 ⁻²	0.19	1.01 x 10 ⁻¹
6	5.94 x 10 ⁻²	1.96	2.21 x 10 ⁻²	0.19	4.44 x 10 ⁻²
8	4.61 x 10 ⁻²	1.48	2.12 x 10 ⁻²	0.19	2.53 x 10 ⁻²
10	3.81 x 10 ⁻²	1.19	1.97 x 10 ⁻²	0.18	1.61 x 10 ⁻²
12	3.37 x 10 ⁻²	9.81 x 10 ⁻¹	1.71 x 10 ⁻²	0.16	1.20 x 10 ⁻²
14	2.92 x 10 ⁻²	8.45 x 10 ⁻¹	1.41 x 10 ⁻²	0.15	6.82 x 10 ⁻³
16	2.61 x 10 ⁻²	7.38 x 10 ⁻¹	1.09 x 10 ⁻²	0.12	4.87 x 10 ⁻³
18	2.21 x 10 ⁻²	6.54 x 10 ⁻¹	8.29 x 10 ⁻³	0.10	2.25 x 10 ⁻³
20	1.84 x 10 ⁻²	5.88 x 10 ⁻¹	6.27 x 10 ⁻³	0.09	1.14 x 10 ⁻³
22	1.66 x 10 ⁻²	5.34 x 10 ⁻¹	4.82 x 10 ⁻³	0.08	5.76 x 10 ⁻⁴
24	1.54 x 10 ⁻²	4.89 x 10 ⁻¹	3.76 x 10 ⁻³	0.07	7.37 x 10 ⁻⁴
26	1.34 x 10 ⁻²	4.52 x 10 ⁻¹	2.98 x 10 ⁻³	0.07	2.12 x 10 ⁻⁴
28	1.11 x 10 ⁻²	4.23 x 10 ⁻¹	2.41 x 10 ⁻³	0.07	4.09 x 10 ⁻³
30	1.07 x 10 ⁻²	3.92 x 10 ⁻¹	1.96 x 10 ⁻³	0.06	1.61 x 10 ⁻⁴
32	9.27 x 10 ⁻³	3.68 x 10 ⁻¹	1.62 x 10 ⁻³	0.06	8.75 x 10 ⁻⁵
34	7.63 x 10 ⁻³	3.47 x 10 ⁻¹	1.36 x 10 ⁻³	0.06	1.29 x 10 ⁻⁴
36	8.21 x 10 ⁻³	3.28 x 10 ⁻¹	1.16 x 10 ⁻³	0.06	8.34 x 10 ⁻⁵
38	9.50 x 10 ⁻³	3.11 x 10 ⁻¹	1.00 x 10 ⁻³	0.05	6.19 x 10 ⁻⁵
40	5.14 x 10 ⁻³	2.97 x 10 ⁻¹	8.59 x 10 ⁻⁴	0.06	8.71 x 10 ⁻⁴
42	7.20 x 10 ⁻³	2.82 x 10 ⁻¹	7.54 x 10 ⁻⁴	0.05	5.84 x 10 ⁻⁵
44	6.25 x 10 ⁻³	2.70 x 10 ⁻¹	6.57 x 10 ⁻⁴	0.05	2.04 x 10 ⁻⁵
46	5.08 x 10 ⁻³	2.59 x 10 ⁻¹	5.73 x 10 ⁻⁴	0.05	2.81 x 10 ⁻⁵
48	7.38 x 10 ⁻³	2.46 x 10 ⁻¹	4.99 x 10 ⁻⁴	0.03	1.11 x 10 ⁻³
50	5.60 x 10 ⁻³	2.38 x 10 ⁻¹	4.27 x 10 ⁻⁴	0.04	2.87 x 10 ⁻⁵
52	6.21 x 10 ⁻³	2.29 x 10 ⁻¹	3.57 x 10 ⁻⁴	0.03	3.83 x 10 ⁻⁵
54	8.90 x 10 ⁻³	2.18 x 10 ⁻¹	2.83 x 10 ⁻⁴	0.00	8.54 x 10 ⁻³
56	5.96 x 10 ⁻³	2.14 x 10 ⁻¹	2.13 x 10 ⁻⁴	0.02	2.74 x 10 ⁻⁵
58	8.56 x 10 ⁻⁴	2.09 x 10 ⁻¹	1.50 x 10 ⁻⁴	0.03	1.65 x 10 ⁻³
60	1.52 x 10 ⁻¹⁷	1.95 x 10 ⁻¹	9.92 x 10 ⁻⁵	0.00	1.39 x 10 ⁻³
62	4.16 x 10 ⁻¹⁷	1.90 x 10 ⁻¹	6.71 x 10 ⁻⁵	0.00	4.67 x 10 ⁻⁵
64	9.48 x 10 ⁻¹⁷	1.83 x 10 ⁻¹	4.28 x 10 ⁻⁵	0.00	2.94 x 10 ⁻³
66	2.61 x 10 ⁻¹⁶	1.79 x 10 ⁻¹	2.85 x 10 ⁻⁵	0.00	1.69 x 10 ⁻⁵
68	1.32 x 10 ⁻²	1.74 x 10 ⁻¹	1.85 x 10 ⁻⁵	0.00	2.25 x 10 ⁻³

Table S11. A list of high performing Dy-based SMMs examined in this study. Asterisk indicates parameters from magnetically dilute samples. T_{B1} = ZFC peak, T_{B2} = 100 s relaxation time and T_H = open hysteresis temperature.

	U_{eff}/K	$\tau_0 \times 10^{-12}/\text{s}$	$C/\text{s}^{-1}\text{K}^{-n}$	n	τ_{QTM}/s	T_{B1}/K	T_H/K	T_{B2}/K	$\tau_{\text{Switch}}/\text{s}$	<i>ref</i>
[Dy(Cp*)(Cp(iPr) ₅)][B(C ₆ F ₅) ₄]	2217	4.2	3.1×10^{-8}	3	25000	52	80	67	48.6	S8
[Dy{Cp(iPr) ₄ (Me)} ₂][B(C ₆ F ₅) ₄]	2112	4.01	1.57×10^{-6}	2.07	2452	45	72	64	54.5	S9
[Dy{Cp(iPr) ₅ } ₂][B(C ₆ F ₅) ₄]	1919	11.8	8.04×10^{-7}	2.31	447	42	66	59	38.4	S9
[Dy(Cp ^{ttt}) ₂][B(C ₆ F ₅) ₄]*	1754	20.6	4.29×10^{-6}	1.88		40	60	56	60.0	S10
[Dy{Cp(iPr) ₄ (Et)} ₂][B(C ₆ F ₅) ₄]	1986	7.79	3.36×10^{-8}	3.02	1187	30	66	57	50.4	S9
[Dy{Cp(iPr) ₄ } ₂][B(C ₆ F ₅) ₄]	1848	3.39	2.27×10^{-5}	2	439	19	32	18	5.91	S9
[Dy(O ^t Bu) ₂ (ppy) ₅][BPh ₄]	1815	1.17	1×10^{-6}	3.77		14	4	12	6.04×10^{-2}	S11
[Dy(bbpen)Br]*	1191	0.271	1.75×10^{-5}	4.2	0.04	8	5	-	2.21×10^{-3}	S12
[Dy(DiMeQ) ₂ Cl ₃ (H ₂ O)]*	1110	2	6×10^{-4}	3.89	1.2	6	5	-	1.40×10^{-4}	This Work

References

- S1. a) G. M. Sheldrick, SADABS, empirical absorption correction program based upon the method of Blessing; b) L. Krause, R. Herbst-Irmer, G. M. Sheldrick, D. Stalke, *J. Appl. Cryst.* **2015**, *48*, 3–10. (c) R. H. Blessing, *Acta Crystallogr.* 1995, **A51**, 33–38.
- S2. a) G. M. Sheldrick, *Acta Crystallogr.*, 2015, **C71**, 3–8; b) O. V. Dolomanov, L. J. Bourhis, R. J. Gildea, J. A. K. Howard, H. Puschmann, *J. Appl. Cryst.*, 2009, **42**, 339–341
- S3. M. Pinsky and D. Avnir, *Inorg. Chem.*, 1998, **37**, 5575–5582.
- S4. F. Aquilante, J. Autschbach, R. K. Carlson, L. F. Chibotaru, M. G. Delcey, L. De Vico, I. Fdez. Galván, N. Ferré, L. M. Frutos, L. Gagliardi, M. Garavelli, A. Giussani, C. E. Hoyer, G. Li Manni, H. Lischka, D. Ma, P. Å. Malmqvist, T. Müller, A. Nenov, M. Olivucci, T. B. Pedersen, D. Peng, F. Plasser, B. Pritchard, M. Reiher, I. Rivalta, I. Schapiro, J. Segarra-Martí, M. Stenrup, D. G. Truhlar, L. Ungur, A. Valentini, S. Vancoillie, V. Veryazov, V. P. Vysotskiy, O. Weingart, F. Zapata and R. Lindh, *J. Comput. Chem.*, 2016, **37**, 506–541.
- S5. a) B. O. Roos, R. Lindh, P.-Å. Malmqvist, V. Veryazov and P.-O. Widmark, *J. Phys. Chem. A*, 2004, **108**, 2851–2858; b) B. O. Roos, R. Lindh, P.-Å. Malmqvist, V. Veryazov and P.-O. Widmark, *J. Phys. Chem. A*, 2005, **109**, 6575–6579.
- S6. L. Ungur and L. F. Chibotaru, *Chem. Eur. J.*, 2017, **23**, 3708–3718.
- S7. N. F. Chilton, D. Collison, E. J. L. McInnes, R. E. P. Winpenny and A. Soncini, *Nature Commun.*, 2013, **4**, 2551.
- S8. F. Guo, B. M. Day, Y. Chen, M. Tong, A. Mansikkämäki and R. A. Layfield, *Science.*, 2018, **362**, 1400–1403.
- S9. K. R. McClain, C. A. Gould, K. Chakarawet, S. J. Teat, T. J. Groshens, J. R. Long and B. G. Harvey, *Chem. Sci.*, 2018, **9**, 8492–8503.
- S10. C. A. P. Goodwin, F. Ortú, D. Reta, N. F. Chilton and D. P. Mills, *Nature*, 2017, **548**, 439–442.
- S11. Y.-S. Ding, N. F. Chilton, R. E. P. Winpenny and Y.-Z. Zheng, *Angew. Chemie Int. Ed.*, 2016, **55**, 16071–16074.
- S12. J. Liu, Y.-C. Chen, J.-L. Liu, V. Vieru, L. Ungur, J.-H. Jia, L. F. Chibotaru, Y. Lan, W. Wernsdorfer, S. Gao, X.-M. Chen and M.-L. Tong, *J. Am. Chem. Soc.*, 2016, **138**, 5441–5450.